

WIYN OPEN CLUSTER STUDY. XXXVIII. STELLAR RADIAL VELOCITIES IN THE YOUNG OPEN CLUSTER M35 (NGC 2168)

AARON M. GELLER*, ROBERT D. MATHIEU*, ELLA K. BRADEN*, SØREN MEIBOM*.[†]
 Department of Astronomy, University of Wisconsin - Madison, WI 53706, USA

AND

IMANTS PLATAIS
 Department of Physics and Astronomy, The Johns Hopkins University, Baltimore, MD 21218, USA

AND

CHRISTOPHER J. DOLAN*
 Department of Astronomy, University of Wisconsin - Madison, WI 53706, USA

ABSTRACT

We present 5201 radial-velocity measurements of 1144 stars, as part of an ongoing study of the young (150 Myr) open cluster M35 (NGC 2168). We have observed M35 since 1997, using the Hydra Multi-Object Spectrograph on the WIYN 3.5m telescope. Our stellar sample covers main-sequence stars over a magnitude range of $13.0 \leq V \leq 16.5$ ($1.6 - 0.8 M_{\odot}$) and extends spatially to a radius of 30 arcminutes (7 pc in projection at a distance of 805 pc or ~ 4 core radii). Due to its youth, M35 provides a sample of late-type stars with a range of rotation periods. Therefore, we analyze the radial-velocity measurement precision as a function of the projected rotational velocity. For narrow-lined stars ($v \sin i \leq 10 \text{ km s}^{-1}$), the radial velocities have a precision of 0.5 km s^{-1} , which degrades to 1.0 km s^{-1} for stars with $v \sin i = 50 \text{ km s}^{-1}$. The radial-velocity distribution shows a well-defined cluster peak with a central velocity of $-8.16 \pm 0.05 \text{ km s}^{-1}$, permitting a clean separation of the cluster and field stars. For stars with ≥ 3 measurements, we derive radial-velocity membership probabilities and identify radial-velocity variables, finding 360 cluster members, 55 of which show significant radial-velocity variability. Using these cluster members, we construct a color-magnitude diagram for our stellar sample cleaned of field star contamination. We also compare the spatial distribution of the single and binary cluster members, finding no evidence for mass segregation in our stellar sample. Accounting for measurement precision, we place an upper limit on the radial-velocity dispersion of the cluster of $0.81 \pm 0.08 \text{ km s}^{-1}$. After correction for undetected binaries, we derive a true radial-velocity dispersion of $0.65 \pm 0.10 \text{ km s}^{-1}$.

(galaxy:) open clusters and associations: individual (NGC 2168) - (stars:) binaries: spectroscopic

1. INTRODUCTION

Young open clusters are laboratories for the direct study of the near-primordial characteristics of stellar populations. Their properties, and particularly those of the binary systems, offer unique insights into how stars are born and provide essential guidance for N -body studies of star clusters. Indeed, with sophisticated N -body simulations now able to model real open clusters (e.g., Hurley et al. 2005), knowledge of the correct initial conditions are all the more important. In particular, the initial binary population has a vast impact on the dynamical evolution of the cluster, and the characteristics of the initial binary population will affect the overall frequency, formation rate and formation mechanisms of anomalous stars, like blue stragglers, as interactions with binaries are thought to be catalysts for the formation of these exotic objects (Hurley et al. 2005; Knigge et al. 2009). As a rich open cluster with an age of ~ 150 Myr, M35 is a prime cluster to define these hitherto poorly known initial conditions for the binary population required for any

open cluster simulation.

M35 is a fundamental cluster in the WIYN Open Cluster Study (WOCS; Mathieu 2000), and as such has a strong base of astrometric and photometric observations from both the WOCS collaboration and others. The cluster is centered at $\alpha = 6^{\text{h}}09^{\text{m}}07^{\text{s}}.5$ and $\delta = +24^{\circ}20'28''$ (J2000), towards the Galactic anticenter. Numerous photometric studies have identified the rich main-sequence population (e.g., Kalirai et al. 2003; von Hippel et al. 2002; Sung & Bessell 1999). WOCS CCD photometry places the cluster at a distance of 805 ± 40 pc, with an age of 150 ± 25 Myr, a metallicity of $[\text{Fe}/\text{H}] = -0.18 \pm 0.05$ and a reddening of $E(B - V) = 0.20 \pm 0.01$ (C. Deliyannis, private communication). The most recent published parameters, from Kalirai et al. (2003), place the cluster at a distance of 912_{-65}^{+70} pc ($(m - M)_0 = 9.80 \pm 0.16$) with an age of 180 Myr, adopting a $E(B - V) = 0.20$ and $[\text{Fe}/\text{H}] = -0.21$. (See Kalirai et al. (2003) for a thorough review of previous photometry references and their derived cluster parameters). We note that these two recent studies used different isochrone families.

There have been multiple proper-motion studies of the cluster (Ebbighausen 1942; Cudworth 1971; McNamara & Sekiguchi 1986a), although none determine cluster membership for individual stars fainter than

*Visiting Astronomer, Kitt Peak National Observatory, National Optical Astronomy Observatory, which is operated by the Association of Universities for Research in Astronomy (AURA) under cooperative agreement with the National Science Foundation.

[†]Current address: Harvard-Smithsonian Center for Astrophysics, 60 Garden Street, Cambridge, MA 02138, USA

$V \approx 15.0$. Using proper motions, Leonard & Merritt (1989) derive a cluster mass from 1600-3200 M_{\odot} within 3.75 pc. Detailed observations have also been made in M35 to study tidal evolution in binary stars (Meibom & Mathieu 2005; Meibom et al. 2006, 2007), lithium abundances (Steinhauer & Deliyannis 2004; Barrado y Navascués et al. 2001), and white dwarfs (Reimers & Koester 1988; Williams et al. 2004, 2006, 2009).

This is the first paper in a series studying the dynamical state of M35 through the use of radial-velocity (RV) measurements. The data and results presented in this series will form the largest database of spectroscopic cluster membership and variability in M35 to date. In this paper, we present results from our ongoing radial-velocity study of the cluster, which we began in September 1997. Our stellar sample includes solar-type main-sequence stars within the magnitude range of $13.0 \leq V \leq 16.5$, which corresponds to a mass range¹ of 1.6 - 0.8 M_{\odot} . The main-sequence turnoff is at $V \sim 9.5$, $\sim 4 M_{\odot}$. In Section 2, we describe this stellar sample, observations and data reduction in detail. We thoroughly investigate our RV measurement precision and the effect of stellar rotation in Section 3. Then in Section 4 we derive RV membership probabilities, and use our study of the RV precision to identify RV variables, which we assume to be binaries or higher-order systems. Within this mass range, we identify 360 solar-type main-sequence members; 305 are single² (non-RV-variable) stars while 55 show significant RV variability. We then use these results to plot a color-magnitude diagram (CMD) cleaned of field star contamination, to search for evidence of mass segregation and to study the cluster RV dispersion (Section 5). Finally, in Section 6, we provide a brief summary. In future papers, we will study the binary population of M35 in detail, providing observations that will be used to directly constrain the initial binary population of open cluster simulations.

2. OBSERVATIONS AND DATA REDUCTION

In the following section, we define our stellar sample, provide a detailed description of our observations and data reduction process, and discuss the completeness of our spectroscopic observations.

2.1. Photometric Target Selection

Initially, we created our M35 target list from the stars in three wide-field CCD images centered on M35, taken by T. von Hippel with the Kitt Peak National Observatory (KPNO) Burrell Schmidt telescope on November 18 and 19, 1993. These images have V exposures of 4 s, 20 s and 180 s and B exposures of 4 s, 25 s and 240s covering a $70' \times 70'$ field. We obtained B and V photometry with a limiting magnitude of $V = 17$, denoted as source 1 in

¹ This mass range is derived from a 180 Myr Padova isochrone (Marigo et al. 2008) using the distance, reddening and metallicity from Kalirai et al. (2003).

² In the following, we use the term “single” to identify stars with no significant RV variation. Certainly, many of these stars are also binaries, although generally with longer periods and/or lower mass ratios ($q = m_2/m_1$) than the binaries identified in this study. When applicable, we have attempted to reduce this binary contamination amongst the single star sample by photometrically identifying objects as binaries that lie well above the single-star main-sequence (see Section 4.2).

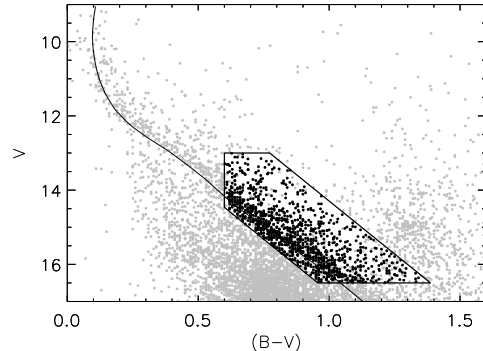


FIG. 1.— Color-magnitude diagram for stars in the field of M35 highlighting the selected region used in this survey. We plot all stars in the field with the gray points to show the location of our selected sample relative to the full cluster. Our stellar sample is bounded by the solid black lines. Within this region, we plot observed stars in the solid black points. Additionally, for reference we plot a 180 Myr Padova isochrone (Marigo et al. 2008) using the distance, reddening and metallicity from Kalirai et al. (2003)

Table 3. Additionally, we derive astrometry from these plates, tied to the Tycho catalogue.

More recently, we added to our database the BV photometry of Deliyannis (private communication), taken on the WIYN³ 0.9m telescope with the S2KB 2K by 2K CCD. This photometry derives from a mosaic of five fields. Each field has a $20' \times 20'$ field-of-view, with one central field and four tiled around the center, for a total field-of-view of $40' \times 40'$. This photometry is denoted as source 2 in Table 3, and covers 74% of the objects we have observed in this study. We note that this photometry is more precise than that of source 1. The star-by-star difference in V magnitudes for the two sources is roughly Gaussian with $\sigma = 0.06$ mag. However there is a tail that extends beyond three times this sigma value. Therefore we caution the reader when using magnitudes from source 1.

We selected stars for the RV master list based on three constraints. The faintest sources that can be observed efficiently at echelle resolution using the Hydra Multi-Object Spectrograph (MOS) on the WIYN 3.5m have $V=16.5$; this therefore sets our faint limit for observations. Stars bluer than $(B-V) \sim 0.6$ ($(B-V)_0 \sim 0.4$) do not provide precise RV measurements due to rapid rotation and paucity of spectral lines; this therefore sets our blue limit for observations. Finally, we perform a photometric selection of cluster member candidates, shown as the outlined region⁴ in Figure 1. This region includes a wide swath above the main sequence so as to not select against binary stars (e.g. Dabrowski & Beardsley 1977), yet also removes stars that are very likely cluster non-members. This photometric selection allows for an efficient survey of the cluster. Our sample extends radially to 30 arcminutes from the cluster center. At a distance of 805 pc, this corresponds to the inner ~ 7 pc of the

³ The WIYN Observatory is a joint facility of the University of Wisconsin-Madison, Indiana University, Yale University, and the National Optical Astronomy Observatories.

⁴ Specifically, we select stars with $0.6 < (B-V) < 1.5$, $13.0 < V < 16.5$ and between the lines defined by $5.7(B-V) + 8.6 < V < 5.7(B-V) + 11.0$.

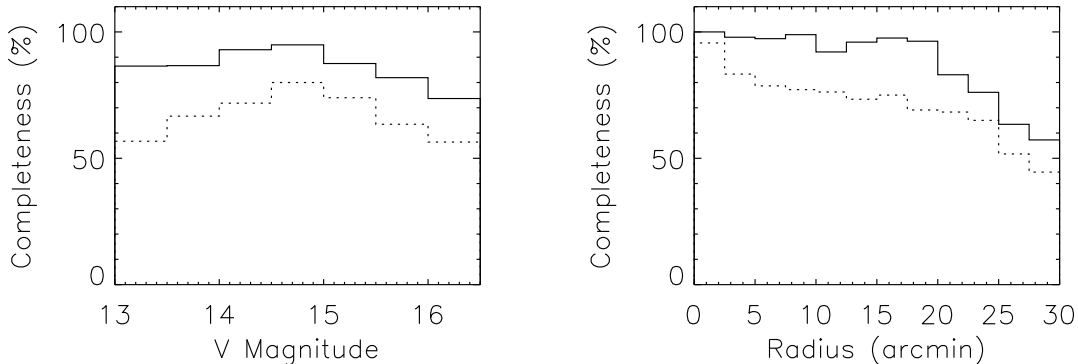


FIG. 2.— Completeness of our observations as a function of V magnitude (left) and projected radius (right). We plot the completeness in stars observed ≥ 3 times with the dashed line, and stars observed ≥ 1 time with the solid line.

cluster in projection. Given the core radius derived by Mathieu (1983) of 1.9 ± 0.1 pc, our sample is drawn from the inner ~ 4 core radii.

Note that we lack BV photometry for $\sim 11\%$ of the point sources found within 30 arcminutes from the cluster center in 2MASS. For most of these objects, it is likely that there is a nearby or overlapping additional object which has prevented accurate BV photometric measurements from either of our sources. These objects, by default, are not included in our stellar sample. In total, our stellar sample contains 1344 stars.

2.2. Spectroscopic Observations

Since September 1997, we have collected 5201 spectra of 1144 stars within this stellar sample as part of an ongoing observing program using the WIYN Hydra MOS. For the majority of these observations, we use Hydra’s blue-sensitive 300 μm fibers, which project to a 3.1’ aperture on the sky. We use the 316 lines mm^{-1} echelle grating, isolating the 11th order with the X14 filter. The resulting spectra span a wavelength range of ~ 25 nm, with a dispersion of 0.015 nm pixel^{-1} , centered on 512.5 nm. We have also occasionally centered our observation on 637.5 nm using a very similar setup. In this region, we use the same grating, but isolate the 9th order with the X18 filter. These observations span a slightly larger wavelength range of ~ 30 nm, and have a dispersion of 0.017 nm pixel^{-1} . Due to a broken filter, observations taken after the spring of 2008 use different observing setups than discussed above; most are centered on 560 nm and all use the echelle grating. We have not noticed any decrease in performance from the new wavelength range, but we caution the reader that we lack sufficient observations in these setups to reliably determine our RV precision for these measurements. During this same period certain upgrades were made to the spectrograph collimator⁵. All observed regions are rich in metal lines. The typical velocity resolution is 15 km s^{-1} . In a two-hour integration, the spectra have signal-to-noise (S/N) ratios ranging from ~ 18 per resolution element for $V=16.5$ stars to ~ 100 per resolution element for $V=13$ stars.

We create fiber configurations (*pointings*) for our observations using a similar method as Geller et al. (2008). Monte Carlo simulations show that we require at least

three observations over the course of a year in order to ensure 90% confidence that a star is either constant or variable in RV out to binary periods of 1000 days (Mathieu 1983, Geller & Mathieu, in preparation). Given three observations with consistent RV measurements over a timespan of at least a year and typically longer, we classify a given star as single (strictly, non-RV variable) and finished, and move it to the lowest priority. If a given star has three RV measurements with a standard deviation > 2.0 km s^{-1} (four times our precision for narrow-lined stars; see Section 4.2), we classify the star as RV variable and give it the highest priority for observation on a schedule appropriate to its timescale of variability. This prioritization allows us to most efficiently derive orbital solutions for our detected binaries.

We place our shortest-period binaries at the highest priority for observations each night, followed by longer-period binaries to obtain 1-2 observations per run. Below the confirmed binaries we place, in the following order, “candidate binaries” (once-observed stars with a RV measurement outside the cluster RV distribution or stars with a few measurements that span only 1.5 - 2.5 km s^{-1}), once observed and then twice observed non-RV-variable likely members, twice observed non-RV-variable likely non-members, unobserved stars, and finally, “finished” stars. Within each group, we prioritize by distance from the cluster center, giving those stars nearest to the center the highest priority. A typical pointing will contain ~ 70 fibers placed on individual stars in our sample and ~ 10 sky fibers.

For a given pointing we obtain three consecutive exposures, each of 40 minutes. In poor transparency or with a particularly bright sky, we restrict the targets to $V < 15.0$ and shorten the integration time, generally to 20 minute exposures. We obtain Thorium-Argon (ThAr), or occasionally Copper-Argon (CuAr), emission-lamp comparison spectra (300 s integrations) before and after each set of science integrations for wavelength calibration and to check for wavelength shifts during the observing sequence. For each set of integrations we also obtain one flat-field image (200 s) of a white spot on the dome illuminated by incandescent lights. Associating the flat-field images with the science integrations is particularly critical for calibrating throughput variations between the fibers in order to apply sky subtractions. In total, we have observed 106 distinct pointings in M35

⁵ http://www.astro.wisc.edu/~mab/research/bench_upgrade/

over the roughly 11 years since our survey began.

2.3. Data Reduction

For a thorough description of our data reduction process, see Geller et al. (2008). In short, we perform a standard bias and flat-field correction to the images using the overscan strip and the flat-field images, respectively. The flat-field spectra are used to trace each aperture in a given pointing and thereby extract the science spectra. Wavelength solutions derived from the emission-lamp spectra are applied, followed by sky-subtraction using sky fibers from each pointing. The three sets of spectra (one set from each integration in a given configuration) are then combined via a median filter to remove cosmic ray signals and improve S/N. These reduced spectra are cross-correlated with a high S/N solar spectrum, obtained using a dusk sky exposure taken on the WIYN 3.5m with the same instrument setup as the given pointing. A Gaussian fit to the cross-correlation function (CCF) yields a RV and a full width at half maximum (FWHM, in km s^{-1}) for each stellar observation. The mean UT time is used to find and correct each RV measurement for the Earth’s heliocentric velocity. Finally we apply the unique fiber-to-fiber RV offsets derived by Geller et al. (2008) for the WIYN-Hydra data to these RVs. As in Geller et al. (2008), to ensure a sufficient quality of measurement, we incorporate into our database only those spectra with a CCF peak height higher than 0.4. Additionally, we examine the distribution of RVs for each individual star and visually inspect any measurements that are outliers in the distribution. Occasionally we remove a measurement whose CCF, though having a peak height above 0.4, clearly provides a spurious measurement (e.g., inadequate sky subtraction).

2.4. Completeness of Spectroscopic Observations

We have at least one observation for 1144 of the 1344 stars in our stellar sample, for a completeness of 85% across our entire sample. 60% of the stars in our stellar sample have sufficient observations for their RVs to be considered final (813/1344). For these stars, we either have ≥ 3 RV measurements that show no variation, or, if we do see RV variability, we have found a binary orbital solution. (These 813 stars comprise the SM, SN, BM and BN classes; see Section 4.1). Of those stars not finalized, 231 have only one or two observations, and another 100 stars are variable but do not yet have definitive orbital solutions.

In Figure 2, we show the completeness of our observations as functions of V magnitude (left) and projected radius (right). We plot the completeness in stars observed ≥ 3 times with the dashed line and stars observed ≥ 1 time with the solid line. Our prioritization of stars by distance from the cluster center is evident by our decreasing completeness towards fainter stars reflects the need for dark skies with minimal sky contamination in order to obtain sufficient S/N in our spectra to derive reliable RVs for faint stars. There are 37 stars with $V < 15$ in our stellar sample that do not have RV measurements, one of which is a proper-motion member. 15 were observed but did not yield reliable RVs, mostly due to rapid rotation.

22 were not observed, 15 of which are farther than 20 arcminutes in radius from the cluster center.

The difference in completeness between bright stars observed ≥ 1 and ≥ 3 times is also a result of an increasing population of rapidly rotating stars towards bluer ($B-V$) color. For many of these stars, we have multiple observations of which only a few, and sometimes one, exceed this cutoff value of CCF peak height >0.4 and therefore are included in our database. For purposes of future research we also include seven rapid rotators in Table 3 for which we have been unable to derive RVs from our spectra.

3. EFFECTS OF STELLAR ROTATION ON MEASUREMENT PRECISION

3.1. Observed Rotation

Because of its youth, M35 provides a sample of late-type stars with a range of rotational periods (Meibom et al. 2009); some of these stars have projected rotational velocities that exceed our spectral resolution. As such, the cluster presents an opportunity to explore empirically the dependence of our measurement precision on increasing $v \sin i$, where i is the inclination angle of the stellar rotation axis to our line of sight.

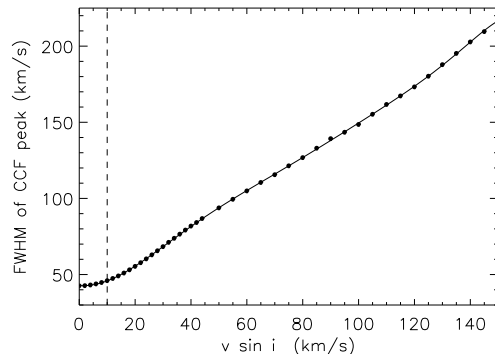


FIG. 3.— FWHM as a function of $v \sin i$ for observations in the 512.5 nm region. FWHM values are measured from the CCF peaks derived from a series of artificially broadened templates, of known $v \sin i$, correlated against the original narrow-lined spectrum. We also show a polynomial fit to the data, which we then use to derive $v \sin i$ values for observed stars in M35. Additionally we plot a dashed line at $v \sin i = 10 \text{ km s}^{-1}$, below which the curve flattens out due to our spectral resolution. We impose a floor in $v \sin i$ at this value as we are unable to reliably measure slower rotation.

The measured FWHM of the CCF for a given star is directly related to the $v \sin i$ (Rhode et al. 2001). Thus in order to derive a $v \sin i$ value, we first measure the FWHM of the CCF peak. To do so, we fit a Gaussian function to the peak, forcing the baseline of the Gaussian to start at the background level of the CCF. Specifically, we subtract from the CCF a polynomial fit to this background level, and then fit the Gaussian to the subsequent “continuum subtracted” CCF. We only use spectra from the 512.5 nm region to measure the FWHM, as the FWHM is dependent on the setup (i.e., the dispersion, etc.), and most of our observations were taken in the 512.5 nm region. We then use a similar technique as Rhode et al. (2001), to convert this FWHM to a $v \sin i$.

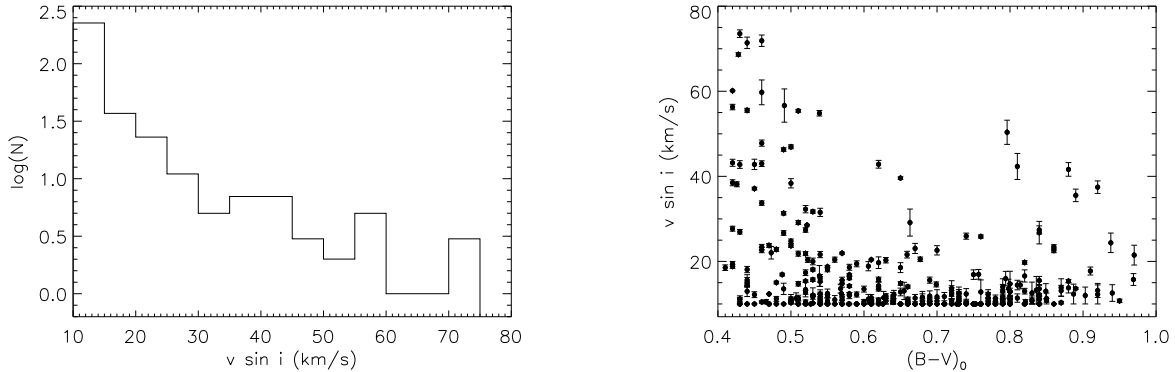


FIG. 4.— Histogram of $v \sin i$ measurements (left) and $v \sin i$ as a function of $(B-V)_0$ (right) for the cluster members of M35. We have removed double-lined binaries and any binaries with known periods less than 10.2 days, the circularization period in M35 (Meibom & Mathieu 2005). We only show stars with mean $v \sin i$ values derived from ≥ 3 observations within the 512.5 nm region. Notice that the stars with the largest rotation are generally also the bluest stars in our sample.

We create a series of artificially broadened templates by convolving our standard solar template with a series of theoretical rotation profiles of specific $v \sin i$ values. We then cross correlate this series of broadened templates with the original narrow-lined template and measure the FWHM of the CCF peak as described above. In Figure 3 we show the results of this analysis along with a polynomial fit to the data. We use this curve to derive $v \sin i$ values for all observations of stars in M35 in the 512.5 nm region. We then take the mean $v \sin i$ for each star, using only our highest quality (CCF peak height > 0.4) spectra, and provide these values in Table 3. We are unable to reliably measure $v \sin i$ values below 10 km s^{-1} , due to the spectral resolution; we therefore impose a floor to the $v \sin i$ at this value.

The median FWHM value that we observe is 46.1 km s^{-1} which corresponds to $v \sin i = 10.3 \text{ km s}^{-1}$. Excluding stars rotating slower than 10 km s^{-1} , we find a precision of 1.4 km s^{-1} for individual $v \sin i$ values of $\leq 25 \text{ km s}^{-1}$, which increases to 1.6 km s^{-1} for $v \sin i > 25 \text{ km s}^{-1}$. These precision values were derived in the same manner as for our RV precision, with a fit to a χ^2 function; see Section 3.2 and Geller et al. (2008). Where possible, we derive a mean $v \sin i$ for a given star from multiple, generally ≥ 3 , observations within the 512.5 nm region. We have compared our $v \sin i$ measurements to the rotation periods from Meibom et al. (2009) for stars observed in both studies, and find the $v \sin i$ and rotation periods to be consistent.

In the left panel of Figure 4, we plot a histogram of the mean $v \sin i$ measurements for M35 cluster members. (See Section 4.1 for our membership criteria.) In this and the other panel, we have excluded any binaries with periods known to be less than the circularization period in M35 of 10.2 days (Meibom & Mathieu 2005), as the rotation of the stars in these binaries have likely been affected by tidal processes. We have also removed any stars that appear to be in double-lined binaries, as the spectral lines in many of these observations are broadened due to the secondary spectrum at similar, though slightly offset, RV. In the right panel of Figure 4, we plot the mean $v \sin i$ as a function of $(B-V)_0$ for M35 cluster members. We see a clear trend of increasing rotation towards bluer stars, as has also been observed in other young open clusters and the field (e.g., field, Hyades, Pleiades,

Kraft 1967; Pleiades, Soderblom et al. 1993; Blanco 1, Mermilliod et al. 2008; IC 2391, Platais et al. 2007).

3.2. Radial-Velocity Precision

We determine the RV measurement precision following Geller et al. (2008), where a χ^2 distribution is fit to the distribution of the standard deviations of the first three RV measurements for each star in an ensemble of stars. Here we do this operation on samples of stars with differing $v \sin i$. Specifically, we consider stars with $v \sin i$ of $\leq 10 \text{ km s}^{-1}$, $10 - 20 \text{ km s}^{-1}$ and $20 - 80 \text{ km s}^{-1}$. The bin sizes were chosen arbitrarily in order to provide sufficiently large samples. The first bin contains all narrow-lined stars for which we have imposed a floor to the $v \sin i$ (see Section 3.1); these stars have line widths characteristic of the auto-correlation of our spectral resolution. The remaining bins contain stars with line widths increased by stellar rotation.

A detailed study of the RV measurement precision of our observation and data-reduction pipeline has been done by Geller et al. (2008) for late-type stars in the old open cluster NGC 188. For the narrow-lined stars in NGC 188 they find a single-measurement precision of 0.4 km s^{-1} . This precision is also a function of the S/N of the spectrum, as shown in Geller et al. (2008) by the degrading precision with increasing V magnitude as well as decreasing CCF peak height. The largest S/N effect seen for narrow-lined stars in NGC 188 is to degrade the precision by 0.25 km s^{-1} . The effect of rotation is larger than this amount. Here, we derive a relationship between the measurement precision and $v \sin i$ and use this relationship in our analysis throughout this paper.

In Figure 5 we show the RV precision as a function of $v \sin i$ in M35 for observations taken in the 512.5 nm region. The narrow-lined stars have a RV precision of 0.5 km s^{-1} , similar to that found for the narrow-lined stars in NGC 188 observed with this same setup. As expected, the value of the measurement precision increases with increasing line width. For the most rapidly rotating stars ($v \sin i > 50 \text{ km s}^{-1}$), the measurement precision degrades to $\sim 1.0 \text{ km s}^{-1}$. We fit a linear relationship to the points in Figure 5, shown as the dashed line:

$$\sigma_i = 0.38 + 0.012(v \sin i) \text{ km s}^{-1}, \quad (1)$$

where σ_i is our precision. We use this equation with the mean measured $v \sin i$ for a given star to calculate

the single-measurement RV precision for that star. We adopt a floor to our precision at 0.5 km s^{-1} , as found for our narrow-lined stars, and shown by the break in the dashed line in Figure 5.

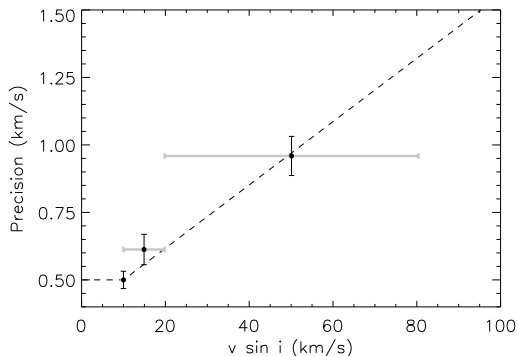


FIG. 5.— RV measurement precision as a function of the average $v \sin i$ (in km s^{-1}) for single lined stars with ≥ 3 observations. The bins are $v \sin i$ of $\leq 10 \text{ km s}^{-1}$, $10 - 20 \text{ km s}^{-1}$ and $20 - 80 \text{ km s}^{-1}$, chosen to provide sufficiently large samples. The gray horizontal bars indicate the bin sizes for each point. The black vertical error bars show the one sigma errors on the precision fit values. The dotted line shows the fit to these data, and provided in Equation 1; we impose a floor to our precision at 0.5 km s^{-1} .

We lack sufficient observations to perform this same analysis using observations in the 637.5 nm region or for observations taken after the spring of 2008 (see Section 2.2). Therefore, for the 129 stars that do not have any observations in the 512.5 nm region ($\sim 11\%$ of our observed stars), we visually inspect the spectra and CCFs. For narrow-lined stars, we set the precision to 0.5 km s^{-1} , and for rotating stars we set the precision to 1.0 km s^{-1} . We can then use this RV precision value for a given star to determine whether our observations for this star are constant or variable in velocity (see Section 4.2). We note that only 13 of these stars have sufficient observations for their RVs to be considered final, and only 2 are probable members.

4. RESULTS

The full M35 database is available with the electronic version of this paper; here we show a sample of our results in Table 3. The first column in Table 3 contains the WOCs identification number (ID_W). These numbers are defined in the same manner as in Hole et al. (2009), with the cluster center set at $\alpha = 6^{\text{h}}9^{\text{m}}7^{\text{s}}.5$ and $\delta = +24^{\circ}20'28''$ (J2000). Next we give the corresponding IDs from Meibom et al. (2009), McNamara & Sekiguchi (1986a) and Cudworth (1971) (ID_M , ID_{Mc} and ID_C). The next few columns provide the right ascension (RA), declination (DEC), the BV photometry and the source number (S) for this photometry (see Section 2.1). Next, we show the number of RV measurements (N) and the mean and standard error of the RV measurements. For stars with only one RV measurements, we show the single-measurement RV precision instead of the standard error. Next we provide this single-measurement RV precision (σ_i , derived using equation 1), the mean and stan-

TABLE 1
GAUSSIAN FIT PARAMETERS FOR CLUSTER
AND FIELD RV DISTRIBUTIONS

	Cluster	Field
Ampl. (Number)	69.0 ± 2.0	2.4 ± 0.4
\overline{RV} (km s^{-1})	-8.17 ± 0.05	13 ± 4
σ (km s^{-1})	0.92 ± 0.08	34 ± 4

dard error of the $v \sin i$ measurements⁶, the e/i value (see Section 4.2), the calculated RV membership probability (P_{RV} , see Section 4.1), the proper-motion membership probability from McNamara & Sekiguchi (1986a) (P_{PM1}) and Cudworth (1971) (P_{PM2}), where available, and then, the classification of the object (see Section 4.3). For RV-variable stars with orbital solutions, we present the center-of-mass (γ) RV with the derived error in place of the mean RV and its standard error, and add the comment SB1 or SB2 for single- and double-lined binaries, respectively. Additionally, for binaries without orbital solutions that appear to be double-lined, we add the comment of SB2. Finally, for purposes of future research we include seven rapid rotators for which we have been unable to derive RVs from our spectra, and label them with the comment RR.

4.1. Membership

The RV distribution of M35 is clearly distinguished from that of the field when we plot a histogram of the mean RVs for the observed stars in our stellar sample. In Figure 6, we show a histogram of the mean RVs for stars with ≥ 3 RV measurements whose standard deviations are $< 2 \text{ km s}^{-1}$, as well as the γ -RVs for binary stars with orbital solutions, thus excluding from the fit any RV variables whose γ -RVs are unknown. The cluster shows a well-defined peak rising above the broad distribution of the field stars. We simultaneously fit one-dimensional Gaussian functions, $F_c(v)$ and $F_f(v)$, to represent the cluster and field RV distributions, respectively, and then use these fits to calculate RV membership probabilities for each individual star. We compute the membership probability $P_{RV}(v)$ with the usual formula:

$$P_{RV}(v) = \frac{F_c(v)}{F_f(v) + F_c(v)} \quad (2)$$

(Vasilevskis et al. 1958). We plot these Gaussian fits in Figure 6 with the dashed lines, and show the fit parameters in Table 1.

For a given single star, we use the mean RV to compute the RV membership probability. For a given binary star with an orbital solution, we compute the RV membership probability from the γ -RV. For RV-variable stars without orbital solutions, the γ -RVs are not known, and therefore we cannot calculate RV membership probabilities. For these stars, we provide a preliminary membership classification, described in Section 4.3.

⁶ For double-lined binaries and stars with no observation in the 512.5 nm region, we do not derive a $v \sin i$ value. For stars with only one measurement in the 512.5 nm region, we convert the 1-sigma error on the FWHM (derived from the Gaussian fit to the CCF peak) to an error on the $v \sin i$ using the fit shown in Figure 3. As this relationship is not linear, we provide the mean of the derived upper and lower errors on $v \sin i$.

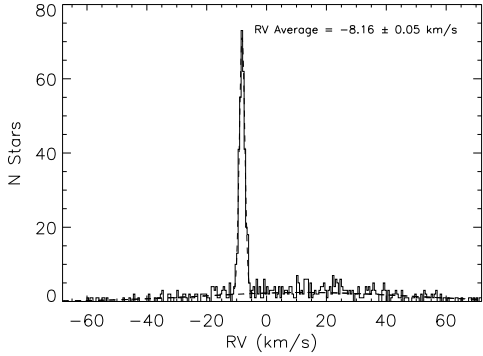


FIG. 6.— RV histogram for stars in the field of M35. We include the mean RVs for stars observed ≥ 3 times with RV standard deviations $< 2 \text{ km s}^{-1}$ and the γ -RVs for binary stars with orbital solutions, excluding RV variables whose γ -RVs are unknown. The bin sizes are 0.5 km s^{-1} , equal to our RV precision for narrow-lined stars, as found in Section 3. The dashed lines show the simultaneous Gaussian fits to the cluster and field RV distributions.

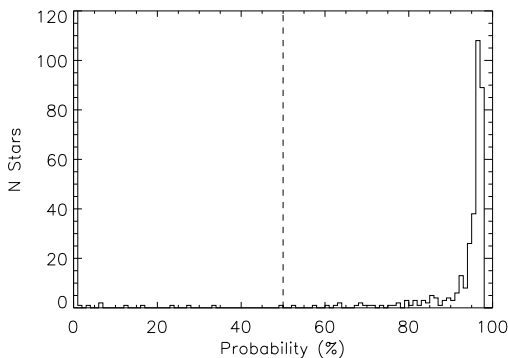


FIG. 7.— Histogram of membership probabilities, P_{RV} , for stars observed ≥ 3 times with RV standard deviations $< 2 \text{ km s}^{-1}$ and for binaries whose γ -RVs are known. For the single stars, we compute P_{RV} using the mean observed RV; for binaries with orbital solutions, P_{RV} is based on the γ -RV. We show our membership cutoff of $P_{RV}=50\%$ with the dashed line, above which we classify a star as a cluster member. Note that we do not show the full height of the bin at lowest membership probability for clarity.

In Figure 7, we show the distribution of RV membership probabilities, displaying a clean separation between the cluster members and field stars. In the following analysis, we use a probability cutoff of $P_{RV} \geq 50\%$ to define our cluster member sample. Using the 344 single cluster members and binary cluster members with orbital solutions, we find a mean cluster RV of $-8.16 \pm 0.05 \text{ km s}^{-1}$. From the area under the fit to the cluster and field distributions, we estimate a field contamination of 6% within our cluster member sample ($P_{RV} \geq 50\%$). Though this estimate is derived excluding the RV variables that do not have orbital solutions, the percent contamination should be valid for the cluster as a whole.

Our RV membership probabilities agree well with the proper-motion memberships of Cudworth (1971) and McNamara & Sekiguchi (1986a). We note that our stellar sample covers only the faintest portion of either proper-motion study. There are 24 Cudworth (1971)

proper-motion members within our observed stellar sample, of which we find 14 (58%) to also have $\geq 50\%$ RV membership probabilities. Cudworth (1971) note that for $V > 13$ they begin to find significant errors in their photometry and expect many field stars to contaminate their proper-motion member sample; this can likely explain the 10 discrepant stars. There are 70 McNamara & Sekiguchi (1986a) proper-motion members within our observed stellar sample, of which we find 64 (91%) to also have $\geq 50\%$ RV membership probabilities. McNamara & Sekiguchi (1986a) expects up to 15 field stars contaminating their cluster member sample from $13 < V < 15$, which can easily account for the 6 discrepant stars.

We also note that NGC 2158 is only ~ 28 arcminutes away from the center of M35, at $\alpha = 6^{\text{h}}07^{\text{m}}25^{\text{s}}$ and $\delta = +24^{\circ}05'48''$ (J2000), and thus is within the spatial region that we have surveyed. Scott et al. (1995) find a mean RV for NGC 2158 of $28 \pm 4 \text{ km s}^{-1}$. There are five stars within our sample that lie within the cluster radius of 2.5 arcminutes Carraro et al. (2002) from the center of NGC 2158 and have RVs within three times the standard error (12 km s^{-1}) of the mean RV : 125044, 39017, 111050, 57037, 54048. Two of these stars (125044 and 57037) have less than three observations; the remaining three have ≥ 3 observations and appear to be non-RV-variables.

4.2. Radial-Velocity Variability

RV-variable stars are distinguishable by the larger standard deviations of their RV measurements. Here, we assume that such velocity variability is the result of a binary companion, or perhaps multiple companions. Specifically, we consider a star to be a RV variable if the ratio of the standard deviation of its RV measurements to the single-measurement RV precision⁷ (e/i) for that star is greater than four (Geller et al. 2008). We provide the e/i value for each single-lined star in Table 3; we label double-lined systems as RV variables directly, and include the comment of SB2 in Table 3.

Monte Carlo analysis has shown that, for similar observations of solar-type stars in NGC 188, Geller & Mathieu (in preparation) can detect the majority of binaries with periods less than 10^4 days and a negligible fraction of longer-period binaries. Though the slightly poorer precision for the M35 data will effect the specific completeness numbers, we can assume a similarly high completeness in detected binaries with periods less than 10^4 days and a corresponding drop in completeness for longer-period binaries. Some of the undetected systems are evident from their separation from the main sequence (see Figure 8).

We have currently identified 55 RV-variable members of M35, and have derived orbital solutions for 71% (39/55) of this sample. In following papers we will provide the orbital solutions for these systems, including all derived parameters. We will then perform a detailed analysis of the distributions of these orbital parameters as well as the binary frequency of the cluster.

⁷ We use the same nomenclature of “ e/i ” as in Geller et al. (2008), though in other sections, for clarity, we have labeled the precision as σ_i , so as not to confuse the precision with an inclination angle.

TABLE 2
NUMBER OF STARS
OR STAR SYSTEMS
WITHIN EACH
MEMBERSHIP
CLASS

Class	Number
SM	305
SN	452
BM	39
BN	17
BLM	16
BU	16
BLN	68
U	231

4.3. Membership Classification of Radial-Velocity Variable Stars

We follow the same classification system as Geller et al. (2008) and Hole et al. (2009) in order to provide a qualitative guide to a given star’s membership and variability, in addition to the calculated RV memberships and e/i values. We provide these classifications for all observed stars, while the memberships and e/i values are only provided for a subset of appropriate stars.

For stars with $e/i < 4$, we classify those with $P_{RV} \geq 50\%$ as single members (SM), and those with $P_{RV} < 50\%$ as single non-members (SN). If a star has $e/i \geq 4$ and enough measurements from which we are able to derive an orbital solution, we use the γ -RV to compute a secure RV membership. For these binaries, we classify those with $P_{RV} \geq 50\%$ as binary members (BM) and those with $P_{RV} < 50\%$ as binary non-members (BN). For RV variables without orbital solutions, we split our classifications into three categories. If the mean RV results in $P_{RV} \geq 50\%$, we classify the system as a binary likely member (BLM). If the mean RV results in $P_{RV} < 50\%$ but the range of measured RVs includes the cluster mean RV, we classify the system as a binary with unknown membership (BU). Finally, if the RV measurements for a given star all lie either at a lower or higher RV than the cluster distribution, we classify the system as a binary likely non-member (BLN), since it is unlikely that any orbital solution could place the binary within the cluster distribution. We classify stars with < 3 RV measurements as unknown (U), as these stars do not meet our minimum criterion for deriving RV memberships or e/i measurements. In the following analysis, we include the SM, BM and BLM stars as cluster members. Including these stars, we find 360 total cluster members in our sample. We list the number of stars within each class in Table 2.

5. DISCUSSION

In the following section, we present a CMD for M35 cleaned of field star contamination (Section 5.1), compare the spatial distribution of the single and binary members (Section 5.2), and analyze the RV dispersion of the cluster (Section 5.3).

5.1. Color-Magnitude Diagram

In Figure 8, we show the CMD for all RV cluster members in M35 from this study for which we have photometry from the WIYN 0.9m, as this set of photom-

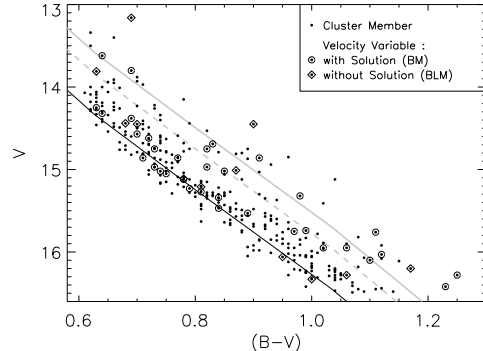


FIG. 8.— Color-magnitude diagram of M35 including only cluster members ($P_{RV} \geq 50\%$) with photometry from WIYN 0.9m (source 2). We plot the RV variables with orbital solutions with circles and without orbital solutions with diamonds. We show the 180 Myr Padova isochrone as the black line. The solid gray line shows where binaries with mass ratios of 1.0 lie on the CMD, and the dashed gray line shows the deviation from the isochrone of twice the photometric error.

etry is of higher precision than that taken on the Burrell Schmidt (see Section 2.1). We also plot a 180 Myr Padova isochrone using the cluster parameters derived by Kalirai et al. (2003) in the black curve. Binaries with orbital solutions are circled and RV variables without orbital solutions are marked by diamonds.

Additionally, we use the Padova isochrone to plot the location on the CMD of binaries with mass ratios $q = 1$, shown as the gray line. We note that there are a number of stars observed brighter and to the red of this line, some that we have not identified as RV variables. In this location on the CMD one would expect to find either higher-order systems or field stars. There are 33 RV members that lie above the $q = 1$ line; 22 are single and 11 show RV variability. We expect a 6% field star contamination within the cluster members sample (Section 4.1). If we include only the 309 cluster members that have photometry from the WIYN 0.9m (and are therefore shown in Figure 8), this results in 19 possible field stars; including our entire cluster member sample results in 22 possible field stars. Therefore field star contamination cannot account for all of these sources, suggesting that a subset of these stars are indeed higher-order systems. We also note that there are an additional 12 cluster members with photometry from the Burrell Schmidt that lie above the $q = 1$ line, but recall that this source of photometry is of poorer precision.

Finally, for use in Sections 5.2, we follow a similar procedure as Montgomery et al. (1993) to attempt to photometrically identify binaries that lie far from the isochrone on the CMD. We derive the distance of each star from the main-sequence isochrone and fit a Gaussian function representing the photometric error distribution to the distribution of these distances. We notice a clear excess in the observed distribution from the Gaussian fit at 2σ , shown as the dashed gray line in Figure 8. We attribute this excess to photometric binaries. A $1 M_{\odot}$ star in M35 with the additional light from a companion of mass-ratio $q = 0.78$ would lie on this line. Therefore sources observed above this line are likely binaries with larger mass ratios ($q > 0.78$), or very infrequently, field stars. We observe 42 cluster members above this line that show

no significant RV variation (and therefore fall into the SM class). Many of these are likely long-period binaries that are outside of our detection limits, as the hard-soft boundary for solar-type stars in M35 is $\sim 10^5 - 10^6$ days, and we only detect binaries with $P \lesssim 10^4$ days (Geller & Mathieu, in preparation).

5.2. Spatial Distribution and Mass Segregation

In Figure 9 we compare the cumulative projected radial distributions of the single and binary projected members of M35. We have attempted to reduce the contamination from undetected binaries within our single-star sample by only including stars with no detectable RV variation (SM) that are fainter and bluer than the dashed gray line in Figure 8. This conservative cut removes large- q (i.e., high total mass) binaries that have periods longer than our detection limit. We have not applied any correction for the spatial bias found in our observations (Section 2.4), because this bias will be present in both the single- and binary-star samples and should therefore not effect this analysis. A Kolmogorov-Smirnov test shows no significant difference between these two populations with a value of 60%. We therefore conclude that the solar-type main-sequence binaries in M35 show no evidence for central concentration as compared to the single stars.

Mathieu (1983) finds a half-mass relaxation time for the cluster of 150 Myr, comparable to the cluster age. This study of the radial spatial distributions for proper-motion-selected member stars in the $8.0 < V < 14.5$ ($\sim 4.4 - 1.2 M_\odot$) range revealed mass segregation only among stars more massive than $2 M_\odot$. The degree of segregation lessens with decreasing mass, and is largely non-existent among solar-like stars. McNamara & Sekiguchi (1986b) found similar results in their proper-motion selected sample, which covered stars down to $V = 14.5$ ($\sim 1.2 M_\odot$). We only include primary stars with masses of $1.6 - 0.8 M_\odot$, and therefore most of our binaries have total masses that are lower than the higher-mass stars that have been shown to be mass segregated. Mathieu (1983) found that M35 is fit well with a multi-mass King model. In such models the reduction in mass segregation for lower-mass systems derives from more severe tidal truncation of higher-dispersion velocity distributions in a cluster potential dominated by the solar-like stars.

5.3. Cluster Radial-Velocity Dispersion

To determine the true RV dispersion of the cluster, we follow the procedure of Geller et al. (2008). We first limit our sample to only include SM stars that have $v \sin i \leq 10 \text{ km s}^{-1}$. We limit the $v \sin i$ value to ensure that we only use the highest precision RV measurements for this analysis. These narrow-lined stars have a precision $\sigma_i = 0.5 \text{ km s}^{-1}$. We will discuss the effect of undetected binaries that likely remain within this sample in Section 5.3.1.

Using this sample of 67 SM stars, we first derive the observed dispersion σ_{obs} by taking the standard deviation of the mean RVs for each star, and we find $\sigma_{obs} = 0.86 \pm 0.07 \text{ km s}^{-1}$. This observed dispersion is a function of our measurement precision and is also inflated by undetected binaries. Therefore, in order to derive the true RV dispersion, we must first account for the precision on these

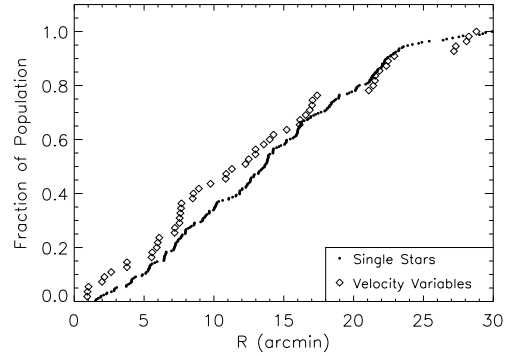


FIG. 9.— Cumulative projected radial spatial distributions of the M35 single and binary cluster members. We have excluded any stars from the single-star sample that are brighter and redder than the dashed gray line in Figure 8, as these stars are likely long-period binaries that are outside of our detection limits. We plot the single stars with the black points and the RV variables with the open diamonds. We find no significant evidence for central concentration of the RV-variable population.

RV measurements. We derive⁸ the “combined RV dispersion” σ_{cb} from :

$$\sigma_{cb}^2 = \sigma_{obs}^2 - \frac{1}{n} \sum_{i=1}^n \xi_i^2. \quad (3)$$

Here, $n = 67$ is the number of stars used in this analysis, and ξ_i is the mean error of the RV for the i th star defined as,

$$\xi_i = \left(\sum_{j=1}^m \frac{(RV_j - \overline{RV}_i)^2}{m(m-1)} \right)^{1/2} \quad (4)$$

where RV_j is one of the m number of RV measurements for a given star i , and \overline{RV}_i is the mean RV for that star. We note that the second term in Equation 3 is very nearly equal to $\sigma_i^2/3$, as we have 3 RVs for most of the stars in this sample, and these narrow-lined stars all have the same precision of $\sigma_i = 0.5 \text{ km s}^{-1}$. Following this procedure, we derive a combined dispersion of $\sigma_{cb} = 0.81 \pm 0.08 \text{ km s}^{-1}$. The error on this combined dispersion is almost entirely due to the statistical error on σ_{obs} .

We find no significant difference in the combined RV dispersion of the SM or BM stars. For the BM stars, we use the γ -RVs in place of the mean RVs, and substitute the measurement precision for the standard deviation portion in Equation 4. There is also no significant variation in the combined RV dispersion as a function of radius, although due to the small sample sizes our binned RV dispersion values have large uncertainties (of $0.1 - 0.15 \text{ km s}^{-1}$ for bins of 10 arcmin).

This combined RV dispersion is inflated by undetected binaries. In the following section, we quantify this effect and apply the correction to derive the true RV dispersion of M35, an improvement on the procedure of Geller et al. (2008).

⁸ The use of Equations 3 and 4 is an improvement over the procedure of Geller et al. (2008) adapted from McNamara & Sanders (1977). The uncertainty on σ_{cb} also follows McNamara & Sanders (1977).

5.3.1. Contribution from Undetected Binaries

The combined RV dispersion defined in Equation 3 is also described by,

$$\sigma_{cb} = \sigma_c + \beta \quad (5)$$

where σ_c is the true RV dispersion of the cluster and β represents the contribution from undetected binaries within our sample. Therefore, in order to derive the true RV dispersion of the cluster we have performed a Monte Carlo analysis to determine this contribution from undetected binaries.

We first create a set of simulated binaries with orbital parameters distributed according to the Galactic field solar-type binaries studied by Duquennoy & Mayor (1991). Specifically, these binaries have a log-normal period distribution centered on $\log(P [\text{days}]) = 4.8$ with $\sigma = 2.3$, and a Gaussian eccentricity distribution centered on $e = 0.3$. For binaries with periods below the circularization period of 10.2 days (Meibom & Mathieu 2005), we set the eccentricity to zero. We use only solar-mass primary stars, and a distribution in secondary mass between $0.08 - 1 M_\odot$ described by a Gaussian centered on $M_2 = 0.23 M_\odot$ with $\sigma = 0.42 M_\odot$ (Kroupa et al. 1990). Duquennoy & Mayor (1991) found this Gaussian to be the best fit to their solar-type field binaries, and this distribution is also consistent with that of Goldberg et al. (2003) for their field binaries with primary masses $> 0.67 M_\odot$. The orbital inclinations and phases of the binaries are chosen randomly. We then generate three RVs for these simulated binaries distributed in time according to the actual distribution of our first three observations for stars in M35. The majority of the SM stars in our sample have only three observations. To these RVs, we also add a random error generated from a Gaussian centered on zero and with $\sigma = 0.5 \text{ km s}^{-1}$, the RV precision for narrow-lined stars in M35. We also add a random velocity offset generated from a Gaussian centered on zero with a standard deviation equal to an adopted one-dimensional RV dispersion.

To this sample, we add a number of simulated single stars to produce a desired binary frequency. We generate three RVs for each single star from a Gaussian described by our precision. To the mean RV for every single star we also add a random offset described by the assumed RV dispersion in the same manner as for the simulated binaries. We then keep only those simulated binaries (and single stars) whose first three RVs result in an $e/i < 4$, and whose mean RVs are within three standard deviations of the mean RV from a Gaussian fit to the simulated RV distribution. This cutoff in standard deviation reflects our membership criterion of $P_{RV} \geq 50\%$ for the M35 observations. These binaries would be undetected within the SM sample.

We then follow the equations given above to derive β for a range of binary frequencies and velocity dispersions, σ_c . In Figure 10, we plot the true cluster RV dispersion (σ_c) as a function of the combined RV dispersion (σ_{cb}) for a range of total binary frequencies, where each line corresponds to a different binary frequency between 0% (far left) to 100% (far right) in steps of 10%. We can then use the results shown in Figure 10 to derive the true RV dispersion for M35. Furthermore, the results shown in this figure are also applicable to RV dispersion

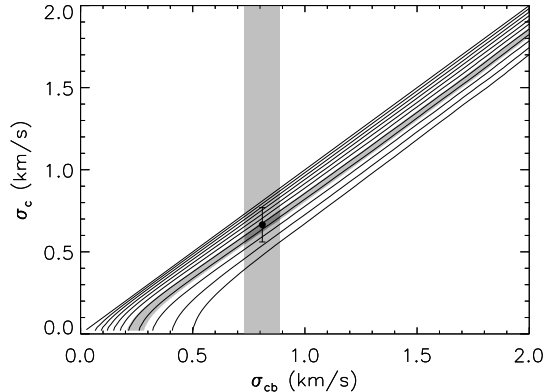


FIG. 10.— The true cluster RV dispersion (σ_c) plotted against the combined RV dispersion (σ_{cb}) for a range of total binary frequencies. Each line corresponds to a different binary frequency in steps of 10%, with 0% at the far left and 100% at the far right. With the vertical gray rectangle, we plot the region included in the combined RV dispersion for M35 of $0.81 \pm 0.08 \text{ km s}^{-1}$. The diagonal gray region covers the possible lines within our extrapolated true binary frequency in M35 of $66\% \pm 8\%$ (derived assuming the M35 binaries follow a Duquennoy & Mayor (1991) period distribution). Finally, we plot the resulting true RV dispersion in M35 of $0.65 \pm 0.10 \text{ km s}^{-1}$ with the black point at the intersection of these two shaded regions.

analyses for other star clusters, provided that the binary population is consistent with the Duquennoy & Mayor (1991) field binaries.

5.3.2. True Radial-Velocity Dispersion

To date, we have detected 55 binaries in M35 out of 360 cluster members. If we assume a similar completeness as in Geller & Mathieu (in preparation), for NGC 188, then we can assume that we have detected 63% of the binaries with periods less than 10^4 days (and a negligible fraction of binaries with longer periods). This correction results in a binary frequency of $24\% \pm 3\%$ for $P < 10^4$ days. This binary frequency is consistent with that of solar-type stars in the Galactic field Duquennoy & Mayor (1991) out to the same period limit. If we assume the M35 binaries follow a Duquennoy & Mayor (1991) period distribution, then our binary frequency for $P < 10^4$ days implies a total binary frequency of $66\% \pm 8\%$, with the inclusion of wider binaries currently beyond our detection limits. We then take this value for the total binary frequency and correct our combined RV dispersion for undetected binaries.

In the filled gray areas in Figure 10 we show the regions defined by our M35 combined RV dispersion and the total binary frequency. At the intersection, we plot the derived true RV dispersion in M35 of $\sigma_c = 0.65 \pm 0.10 \text{ km s}^{-1}$. Using a flat distribution in secondary mass (and mass ratio), as has been suggested by some studies (e.g., Mazeh et al. 1992, 2003), has a negligible effect on the derived true RV dispersion. This true RV dispersion is consistent with the projected velocity dispersion of $1.0 \pm 0.15 \text{ km s}^{-1}$, derived by Leonard & Merritt (1989) using the proper-motion data from McNamara & Sekiguchi (1986a).

6. SUMMARY

This is the first paper in a series studying the dynamical state of the young ($\sim 150 \text{ Myr}$) open cluster M35

(NGC 2168). In this first paper, we present our RV observations and provide initial results from this survey. Our stellar sample extends to 30 arcminutes in radius from the cluster center (7 pc in projection at a distance of 805 pc or ~ 4 core radii), and we have selected a region from a V , $(B-V)$ CMD (Figure 1) which covers a mass range of 1.6 - 0.8 M_{\odot} . We have used the WIYN 3.5m telescope with the Hydra MOS to obtain 5201 spectra of 1144 stars within this stellar sample. From these spectra, we derive RV measurements with a precision of 0.5 km s $^{-1}$ for narrow-lined stars. The vast majority of the observed stars have multiple measurements, allowing determination of cluster membership and identification of spectroscopic binary stars. We detect 360 cluster members, 55 of which show significant variability in their RV measurements. Binary orbital solutions have been obtained for 39 of these RV variables, which we will present in detail in the next paper in this series. Observations of the rest of the RV variables and the remainder of our stellar sample are ongoing. Table 3 provides the first RV membership database for M35 and extends ~ 1.5 magnitudes deeper than any previous membership catalogue.

Using the RV cluster members, we study the spatial distribution and velocity dispersion of the single and binary stars. We find their spatial distributions to be indistinguishable. This lack of central concentration for the binaries is consistent with earlier observational studies of stars in M35 as well as with a fully relaxed dynamical model for the cluster (Mathieu 1983; McNamara & Sekiguchi 1986b). In these studies, mass segregation is seen in higher-mass stars, but diminishes to being undetectable for stars in our observed mass range.

After correcting for measurement precision, but not for binaries, we place an upper limit on the RV dispersion of the cluster of 0.81 ± 0.08 km s $^{-1}$. When we also correct for undetected binaries, we derive a true RV dispersion of 0.65 ± 0.10 km s $^{-1}$.

The WOCS group will continue our survey of M35 in order to derive RV memberships for all stars in our stellar sample and obtain orbital solutions for all binaries with periods less than a few thousand days, as well as some with longer periods. In future papers, we will study the binary population of M35 in detail, providing all orbital solutions and analyzing the binary frequency and distributions of orbital parameters. These data will form essential constraints on the hitherto poorly known initial binary populations used in sophisticated N -body models of open clusters.

The authors would like to express their gratitude to the staff of the WIYN Observatory for their skillful and dedicated work that have allowed us to obtain these excellent spectra. We thank Ata Sarajedini and Ted von Hippel for the acquisition of the Schmidt images, Vera Platais for work on the astrometry and photometry as well as John Bjorkman for early photometry work. We also thank the many undergraduate and graduate students who have contributed late nights to obtain the spectra for this project. This work was supported by NSF grant AST 0406615 and the Wisconsin Space Grant Consortium.

Facilities: WIYN 3.5m

REFERENCES

- Barrado y Navascués, D., Deliyannis, C. P., & Stauffer, J. R. 2001, *ApJ*, 549, 452
- Carraro, G., Girardi, L., & Marigo, P. 2002, *MNRAS*, 332, 705
- Cudworth, K. M. 1971, *AJ*, 76, 475
- Dabrowski, J. P., & Beardsley, W. R. 1977, *PASP*, 89, 225
- Duquenois, A., & Mayor, M. 1991, *A&A*, 248, 485
- Ebbighausen, E. G. 1942, *AJ*, 50, 1
- Geller, A. M., Mathieu, R. D., Harris, H. C., & McClure, R. D. 2008, *AJ*, 135, 2264
- Goldberg, D., Mazeh, T., & Latham, D. W. 2003, *ApJ*, 591, 397
- Hole, K. T., Geller, A. M., Mathieu, R. D., Platais, I., Meibom, S., & Latham, D. W. 2009, *AJ*, 138, 159
- Hurley, J. R., Pols, O. R., Aarseth, S. J., & Tout, C. A. 2005, *MNRAS*, 363, 293
- Kalirai, J. S., Fahlman, G. G., Richer, H. B., & Ventura, P. 2003, *AJ*, 126, 1402
- Knigge, C., Leigh, N., & Sills, A. 2009, *Nature*, 457, 288
- Kraft, R. P. 1967, *ApJ*, 150, 551
- Kroupa, P., Tout, C. A., & Gilmore, G. 1990, *MNRAS*, 244, 76
- Leonard, P. J. T., & Merritt, D. 1989, *ApJ*, 339, 195
- Marigo, P., Girardi, L., Bressan, A., Groenewegen, M. A. T., Silva, L., & Granato, G. L. 2008, *A&A*, 482, 883
- Mathieu, R. D. 1983, Ph.D. thesis (University of California, Berkeley)
- Mathieu, R. D. 2000, in *ASPC*, Vol. 198, "Stellar Clusters and Associations: Convection, Rotation, and Dynamos", ed. R. Pallavicini, G. Micela, & S. Sciortino, 517
- Mazeh, T., Goldberg, D., Duquenois, A., & Mayor, M. 1992, *ApJ*, 401, 265
- Mazeh, T., Simon, M., Prato, L., Markus, B., & Zucker, S. 2003, *ApJ*, 599, 1344
- McNamara, B., & Sekiguchi, K. 1986a, *AJ*, 91, 557
- McNamara, B. J., & Sanders, W. L. 1977, *A&A*, 54, 569
- McNamara, B. J., & Sekiguchi, K. 1986b, *ApJ*, 310, 613
- Meibom, S., & Mathieu, R. D. 2005, *ApJ*, 620, 970
- Meibom, S., Mathieu, R. D., & Stassun, K. G. 2006, *ApJ*, 653, 621
- Meibom, S., Mathieu, R. D., & Stassun, K. G. 2007, *ApJ*, 665, L155
- Meibom, S., Mathieu, R. D., & Stassun, K. G. 2009, *ApJ*, 695, 679
- Mermilliod, J.-C., Platais, I., James, D. J., Grenon, M., & Cargile, P. A. 2008, *A&A*, 485, 95
- Montgomery, K. A., Marschall, L. A., & Janes, K. A. 1993, *AJ*, 106, 181
- Platais, I., Melo, C., Mermilliod, J.-C., Kozhurina-Platais, V., Fulbright, J. P., Méndez, R. A., Altmann, M., & Sperauskas, J. 2007, *A&A*, 461, 509
- Reimers, D., & Koester, D. 1988, *A&A*, 202, 77
- Rhode, K. L., Herbst, W., & Mathieu, R. D. 2001, *AJ*, 122, 3258
- Scott, J. E., Friel, E. D., & Janes, K. A. 1995, *AJ*, 109, 1706
- Soderblom, D. R., Stauffer, J. R., Hudon, J. D., & Jones, B. F. 1993, *ApJS*, 85, 315
- Steinhauer, A., & Deliyannis, C. P. 2004, *ApJ*, 614, L65
- Sung, H., & Bessell, M. S. 1999, *MNRAS*, 306, 361
- Vasilevskis, S., Klemola, A., & Preston, G. 1958, *AJ*, 63, 387
- von Hippel, T., Steinhauer, A., Sarajedini, A., & Deliyannis, C. P. 2002, *AJ*, 124, 1555
- Williams, K. A., Bolte, M., & Koester, D. 2004, *ApJ*, 615, L49
- Williams, K. A., Bolte, M., & Koester, D. 2009, *ApJ*, 693, 355
- Williams, K. A., Liebert, J., Bolte, M., & Hanson, R. B. 2006, *ApJ*, 643, L127

TABLE 3
RADIAL-VELOCITY DATA TABLE

ID_W	ID_M	ID_{Mc}	ID_C	RA	DEC	V	$(B-V)$	S	N	\overline{RV}	RV_e	σ_i	$\overline{v \sin i}$	$(v \sin i)_e$	P_{RV}	P_{PM1}	P_{PM2}	e/i	Class	Comment
96041	410	6:10:28.65	24:11:52.0	16.416	0.960	1	4	51.89	1.55	0.52	11.8	1.1	5.93	BLN	...
36042	209	6:10:34.30	24:14:07.8	14.835	0.859	1	3	-8.74	0.55	0.64	21.6	0.8	96	1.49	SM	...
36045	209	6:10:43.69	24:16:08.9	14.497	0.824	1	17	-9.58	0.19	0.50	10.3	0.2	91	77.46	BM	SB1
138057	366	6:10:50.20	24:04:50.7	16.368	1.165	1	1	-25.13	0.50	0.50	U	...
64052	312	6:10:43.70	24:07:00.8	15.884	1.023	1	4	-8.85	0.64	0.55	14.2	4.2	96	2.34	SM	...
15036	180	...	731	6:10:15.70	24:11:31.7	13.450	0.690	2	1	57.98	0.50	0.50	0	...	U	...
49051	227	6:10:51.32	24:11:10.6	15.086	0.890	1	4	88.83	0.34	0.50	10.0	...	0	1.35	SN	...
29047	87	6:10:44.59	24:13:44.3	14.948	0.895	1	4	56.95	0.28	0.50	10.0	...	0	1.10	SN	...
40032	6:10:11.15	24:14:01.5	15.280	0.820	2	3	-7.72	0.32	0.55	14.3	0.8	96	1.02	SM	...
20037	193	...	758	6:10:22.30	24:14:39.3	14.270	0.650	2	1	3.88	0.50	0.50	7	...	U	...

The contents of each column are defined in Section 4.